Exploring the mechanism of inter-particle charge diffusion

Holger Grosshans[a,*], Miltiadis V. Papalexandris[b]

[a] *Physikalisch-Technische Bundesanstalt (PTB), Bundesallee 100, 38116 Braunschweig, Germany*
[b] *Institute of Mechanics, Materials and Civil Engineering, Université catholique de Louvain, 1348 Louvain-la-Neuve, Belgium*

Abstract

Dispersed solid particles in wall-bounded flows may get electrified during particle-wall collisions due to triboelectric effects. Subsequently, the electrostatic charge migrates from the near-wall regions to the bulk of the flow through the dynamics of the particles (*particle-bound charge transport*) and charge transfer during collisions between particles (*inter-particle charge diffusion*). In this paper, we explore the physics underlying the mechanism of inter-particle charge diffusion, which remains not well understood, by means of numerical simulations. We investigated the efficiency of the charge transport within the particulate phase via this mechanism and propose a time-scale for its characterization for particular systems. The considered parameters of these systems included the particle number density and charge as well as their mechanical and electrical properties. It was found that both an increase of the material density of the particles or of their number density results in an enhanced inter-particle charge diffusion and, thus, a reduction of its time scale. Moreover, if only the number density is high but the material density is kept low, then inter-particle charge diffusion may even become the dominant wall-normal charge transport mechanism. Further, in case some particles carry a high charge they are accelerated towards uncharged particles through electrostatic forces which leads to an efficient charge redistribution.

Keywords: electrostatics, particle dynamics, charge transport, particulate flows

1. Introduction

The capacity of flowing systems to get electrified has been acknowledged long ago during observations of water falls (**??**). Furthermore, this phenomenon can also occur during the filling of tanks and reservoirs with liquids, and it constitutes a hazardous ignition source. In this type of flows, and in wall-bounded flows in general, the charge originates from the formation of an electrical double layer at the solid-liquid interface which leads to a diffuse charge layer in the liquid. It is well-known that the extent of the charging of the fluid is strongly influenced by its flow pattern (**??**). More specifically, if the flow is laminar or the thickness of the diffuse layer (also referred to as the *Debye length*) is smaller than the viscous sublayer, then the diffuse layer is not affected by the flow turbulence. Thus, the charge remains confined within a thin layer in near-wall region. On the other hand, if the flow is turbulent and the viscous sublayer is thinner than the diffuse layer, turbulent structures penetrate the diffuse layer and transport charge from the wall towards the bulk of the flow. This results in a significant increase of the total charge accumulation of the fluid.

Moreover, if solid particles made of a material different than the material of the wall are transported by a carrier fluid, then the fluid-solid mixture might be additionally electrified through triboelectrification. This phenomenon is also known as *contact charging* (**?**). The elucidation of the physics of triboelectric charging was subject of various research efforts in the past decades (see e.g. **????**). On the other hand, if two solid objects are made of the same material, then charge exchange between them is typically observed only if they carry different amounts of charge prior to contact. In this case, the pre-charge located at the surface of one object is partially transferred to the surface of the other object. A computational model for this charge exchange between particles of the same material was presented by **?** focusing on aerosols in the atmosphere.

We remark that both phenomena occur during the flow of particles over a solid surface. Examples include sandstorms (**?**), polls on plant surfaces (**?**) and

*Corresponding author
Email address: holger.grosshans@ptb.de (Holger Grosshans)

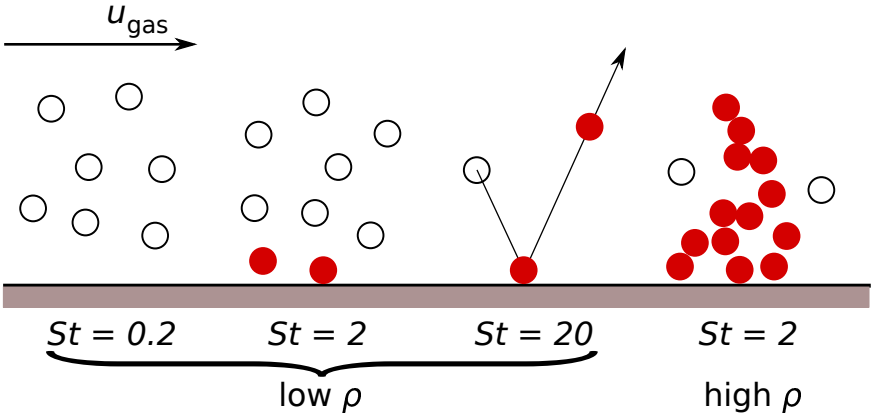

Figure 1: Mechanisms of charge generation and transport in a wall-bounded flow of a fluid-solid mixture depending on the particles Stokes number and number density according to **?**. The red color indicates charged particles. The charge is transported towards the bulk of the flow through particle-bound charge transport ($St \gg 1$, low ρ) or inter-particle charge diffusion ($St = 2$, high ρ).

pneumatic transport of powders in process industries (**?????**). Similar to the above described charging of a liquid, the electrification of the flow takes place in the region of a very thin layer in the vicinity of the surface, i.e. where the particles collide with the solid surface. Subsequently, the charge is transported away from the surface towards the bulk of the fluid-solid mixture flow.

In a previous paper (**?**), we identified the fundamental mechanisms underlying the charge generation and transport within a fluid-solid mixture. With respect to charge transport, we have identified four cases, which are depicted schematically in figure 1. These cases are characterized by the particles' Stokes number, St, and number density, ρ. The former is defined as the ratio between the particle response time and the characteristic time-scale of the fluid flow whereas the latter denotes the number of particles per unit volume. Our numerical results demonstrated the crucial role of the phenomenon turbophoresis, *i.e.* the tendency of particles to migrate in the direction of decreasing turbulent intensity (**??**), on the charging process. **More specifically, for the case of $St = 0.2$ and a low value of ρ, which is depicted in the left of figure 1, particle inertia is too low to allow the particles to cross the turbulent structures close to the wall. Consequently, turbophoresis diminishes particle-wall collisions and reduces charging significantly. An intermediate Stokes number (second case) results in an increased particle inertia which enables the particles to overcome small-scale turbulence structures, collide with the wall and get charged.** However, turbophoresis prevents the migration of the particles towards the bulk of the flow. Thus, the charge remained confined in a layer close to the wall.

An effective charge transport in the wall normal direction takes place if the Stokes number is further increased ($St = 20$, third case). There, the particles have sufficient inertia to convect the charge they carry, which we termed *particle-bound charge transport*. However, we found that for intermediate Stokes numbers the charge may also migrate towards the bulk of the flow as long as the particle number density is sufficiently high (fourth case), (**?**). Contrary to particle-bound charge transport, the latter mechanism does not require a strong particle mobility to efficiently transport charge. Instead, the charge is transported in space through charge exchange in between particles during collisions. Due to the analogy to other diffusion processes, we called this mechanism *inter-particle charge diffusion*. The addressed analogy relates to the random motion of particles, caused by the turbulence of the carrier phase, and the exchange of a property via collisions between particles which is also a feature of e.g. heat or momentum diffusion.

However, despite having identified the existence of inter-particle charge diffusion in particulate flows with high particle number densities (**?**), this mechanism has not been studied in detail yet. The objective of this paper is to investigate under which conditions this particular mechanism becomes important. To this end, we have set up a simplified mathematical model, neglecting fluid forces on the particles and focusing on the charge transfer during inter-particle collisions, which we describe in the following section. This model can be seen as a learning model to understand an elementary component of a complex multi-physics system. In section 3 we present

and discuss our results based on this model. Finally, our conclusions are provided in the last section.

2. Mathematical model

The trajectory of each particle was computed individually in a Lagrangian framework. In order to focus on the interplay between generic particle dynamics and inter-particle charge diffusion, independent of specific flow situations, we considered a gravitation-free vacuum. Thus, the acceleration of an electrically charged particle is given by

$$\frac{\mathrm{d}\boldsymbol{u}_\mathrm{p}}{\mathrm{d}t} = \boldsymbol{f}_\mathrm{coll} + \boldsymbol{f}_\mathrm{el}\,, \tag{1}$$

where $\boldsymbol{u}_\mathrm{p}$ is the particle velocity and $\boldsymbol{f}_\mathrm{coll}$ and $\boldsymbol{f}_\mathrm{el}$ its acceleration due to potential collisions and a present electric field, respectively.

The collisional acceleration term accounts for both inter-particle and particle-wall collisions which are considered to be fully elastic and binary. More specifically, in case of the collision between two particles (denoted by the indices i and n) of the radii $r_{\mathrm{p},i}$ and $r_{\mathrm{p},n}$ and the velocities $\boldsymbol{u}_{\mathrm{p},i}$ and $\boldsymbol{u}_{\mathrm{p},n}$, the post-collision velocity of particle i, $\boldsymbol{u}'_{\mathrm{p},i}$, reads

$$\boldsymbol{u}'_{\mathrm{p},i} = \frac{r^3_{\mathrm{p},i}\boldsymbol{u}_{\mathrm{p},i} + r^3_{\mathrm{p},n}\boldsymbol{u}_{\mathrm{p},n} + r^3_{\mathrm{p},n}(\boldsymbol{u}_{\mathrm{p},n} - \boldsymbol{u}_{\mathrm{p},i})}{r^3_{\mathrm{p},i} + r^3_{\mathrm{p},n}}\,. \tag{2}$$

Further, the post-collision velocity of a particle upon impact with the wall is computed via the relations

$$\boldsymbol{u}''_\mathrm{p} \cdot \boldsymbol{n}_\parallel = \boldsymbol{u}_\mathrm{p} \cdot \boldsymbol{n}_\parallel\,, \tag{3}$$

$$\boldsymbol{u}''_\mathrm{p} \cdot \boldsymbol{n}_\perp = -\boldsymbol{u}_\mathrm{p} \cdot \boldsymbol{n}_\perp\,. \tag{4}$$

In the above equations, $\boldsymbol{n}_\perp$ and $\boldsymbol{n}_\parallel$, denote the unit vectors perpendicular and tangential to a wall.

The force due to an electric field acting on the n-th particle is the sum of the Coulomb forces from the other $N-1$ present particles, i.e.

$$\boldsymbol{f}_{el,n} = \sum_{i=1,i\neq n}^{N} \frac{Q_n\, Q_i\, \boldsymbol{z}_{i,n}}{4\,\pi\,\varepsilon\, m_{\mathrm{p},n}\,|\boldsymbol{z}_{i,n}|^3}\,. \tag{5}$$

In the above equation, Q is the electric charge of the particles and m_p is their mass. The permittivity of the ambient medium is denoted by ε which is in the present study equal to the one of vacuum, namely $\varepsilon = 8.854 \times 10^{-12}$ F/m. Further, $\boldsymbol{z}_{i,n}$ is a vector pointing from the center of particle i to the center of particle n. According to the above formulation, we accounted for the absolute particle charges and neglected charges induced at the surface.

Inter-particle charge exchange occurs when the particles collide with each other. In the present study we considered particles of a homogeneous material, i.e. of identical work functions and resistivities. Thus, triboelectric effects are absent when particles are in contact with each other. Consequently, no charge exchange occurs during collisions between equally charged particles.

However, inter-particle charge exchange takes place if two colliding particles carry different charges prior to the collision. To compute the amount of transferred charge we employed the model of (**?**) which is based on an analogy to the charging of a capacitor. Accordingly, the charge exchanges, ΔQ_i and ΔQ_n, during particle-particle collisions were calculated by

$$\Delta Q_i = -\Delta Q_n = \frac{C_i C_n}{C_i + C_n}\left(\frac{Q_n}{C_n} - \frac{Q_i}{C_i}\right)\left(1 - \mathrm{e}^{-\Delta t_{i,n}/T_{i,n}}\right)\,, \tag{6}$$

In the above equation, $\Delta t_\mathrm{i,n}$ is the contact time during the collision, C_i and C_n are the electric capacities of the two involved particles, and $T_\mathrm{i,n}$ is the charge relaxation time.

The electric capacity of particle i of the radius $r_{\mathrm{p},i}$ was calculated as follows,

$$C_i = 4\,\pi\,\varepsilon\, r_{\mathrm{p},i}\,. \tag{7}$$

Further, the charge relaxation time $T_\mathrm{i,n}$ is given by

$$T_\mathrm{i,n} = \frac{C_i C_n}{C_i + C_n}\frac{r_{\mathrm{p},i} + r_{\mathrm{p},n}}{A_{i,n}}\varphi\,, \tag{8}$$

where the resistivity of the particles' surface is φ. The contact area $A_{i,n}$ was calculated according to the elastic theory of Hertz as

$$A_{i,n} = \frac{\pi\, r_{\mathrm{p},i}\, r_{\mathrm{p},n}}{r_{\mathrm{p},i} + r_{\mathrm{p},n}}\alpha\,, \tag{9}$$

with

$$\alpha = r_{\mathrm{p},i}\, r_{\mathrm{p},n}\left(\frac{5}{8}\,\pi\,\rho_\mathrm{p}\,|\boldsymbol{u}_\mathrm{p,rel}|^2\,\frac{\sqrt{r_{\mathrm{p},i} + r_{\mathrm{p},n}}}{r^3_{\mathrm{p},i} + r^3_{\mathrm{p},n}}\,\gamma_\mathrm{p}\right)^{2/5}\,. \tag{10}$$

In the last expression, $\boldsymbol{u}_\mathrm{p,rel}$ is the relative velocity of the two colliding particles and ρ_p their material density. Further, the elasticity parameter γ_p is defined as

$$\gamma_\mathrm{p} = \frac{1 - \mu^2_\mathrm{p}}{E_\mathrm{p}} \tag{11}$$

where μ_p and E_p are the Poisson ratio and the Young modulus, respectively, of the material of the particles. Finally, the duration of the particle contact, $\Delta t_{i,n}$, was also calculated by the theory of Hertz as follows,

$$\Delta t_{i,n} = \frac{2.94}{|\boldsymbol{u}_\mathrm{p,rel}|}\alpha\,. \tag{12}$$

3. Results and Discussion

First, we **checked the correct implementation** of the mathematical model described in section 2. For the sake of clarity and on the grounds of availability of reference data, the model describing the dynamics of a charged particle in an electric field (equations (1) and (5)) and the charge exchange model (equations (6) – (12)) were treated separately. The former was effectuated by comparing the dynamics of a single particle influenced by the electric field of another charged particle to analytical solutions as proposed by (**?**).

According to the principle of energy conservation the sum of the particle's kinetic energy, W_kin, and its potential electrostatic energy, W_pot, given by

$$W_\mathrm{kin} = \frac{2}{3}\,\pi\,\rho_\mathrm{p}\,r_\mathrm{p}^3\,u_\mathrm{p}^2 \quad \text{and} \quad W_\mathrm{pot} = \frac{Q_1\,Q_2}{4\,\pi\,\varepsilon\,x}\,, \tag{13}$$

remains constant in time. In the above equations, u_p is the particle's velocity, Q_1 and Q_2 is the charge carried by both particles and x is the spacing in between them.

In the considered setting we released particle 1 of the radius $r_\mathrm{p} = 250$ µm and a density of $\rho_\mathrm{p} = 4000$ kg/m^3 at initial rest in the distance of $x_0 = 5$ mm from an immobile second particle. Both particles carried the same charge, $Q = Q_1 = Q_2$. Inserting the initial conditions in equation (13) and solving this relation for the particle velocity in radial direction from the immobile charge, u_p, yields

$$u_\mathrm{p} = \left(\frac{3\,Q^2}{8\,\pi^2\,\varepsilon\,\rho_\mathrm{p}\,r_\mathrm{p}^3}\left(\frac{1}{x_0} - \frac{1}{x}\right)\right)^{0.5}\,. \tag{14}$$

In figure 2 both the numerically and analytically through equation (14) derived particle trajectories are given. Three different charges were calculated, namely Q = 50 pC, 100 pC and 200 pC. Due to the higher electrostatic repulsive forces, the more particle accelerates, the higher the particle charge becomes. The comparison of the three cases shows that the analytical and numerical results agree very well. Thus, of equations (1) and (5) that describe the particle dynamics **are correctly implemented**.

Concerning the charge exchange between dissimilar materials, we have previously successfully **compared** our solver with the experimentally measured charge which is accumulated by a complete powder when transported pneumatically through a pipe (cf. **??**). However, owing to the complexity of the involved physical processes there is currently no suitable experimental data or analytical expression available to compare the model of the charge transfer between particles of the same material during their collision (cf. equations (6) – (12)) with. In fact, according to the well-known tribolelectric series (see e.g. **?**), no triboelectric charging should take place and only possible pre-charge of the particles is exchanged. However, large differences in the triboelectric behavior between samples of different and even nominally the same material are commonly observed in experiments (**???**). Thus, the model given by equations (6) – (12) can be considered as a representation of one possible scenario. Given these points,

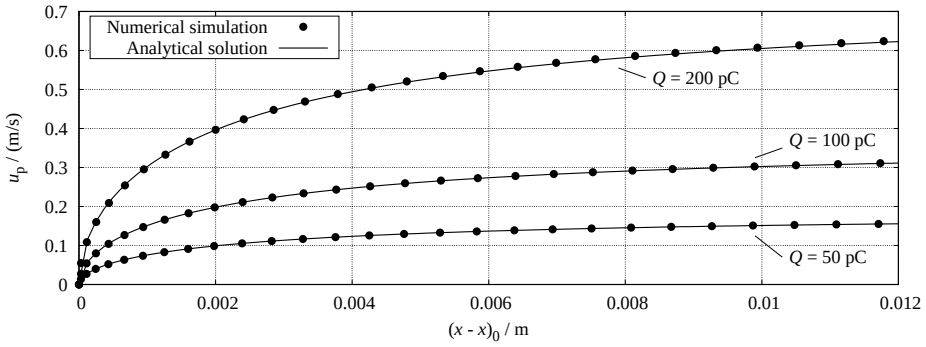

Figure 2: Comparison of numerically and analytically (through equation 14 derived) particle trajectories. The particles are of the radius $r_\mathrm{p} = 250$ µm and a density of $\rho_\mathrm{p} = 4000$ kg/m^3.

we employed the implementation of the mathematical model of section 2 to investigate the mechanism of inter-particle charge diffusion as presented in the following.

Analyzing the system of equations, one may note that a large amount of parameters is investigated. Therefore, it is evident that we cannot study all parameters as well as their interactions. Henceforth, we present in the following the most relevant dependencies and relationships in-between them. The parameters can be organized in three groups. The first one includes γ and φ which appear only in the equations of the charge exchange model and not directly in the equations for the particle dynamics. Further, they relate only to the material properties and are constant for a certain type of particles. Thus, they were investigated independently from the other quantities. The second group defines the frequency of interaction between particles. This group consists of ρ and u_0 where the latter denotes the initial particle velocity. In order to study the influence of the interaction frequency, we let ρ vary. On the other hand, the initial velocity was kept constant, $u_0 = 0.5$ m/s. The second group relates to the question whether an interaction between particles leads to a collision, i.e. charge exchange between both, or if their repelling forces due to their charge prevent contact. We demonstrated in **?** that this group involves ρ, ρ_p, Q, r_p and u_0. To gain insight in the influence of this group we varied additionally ρ_p and Q while the particle radius is treated constant, $r_\mathrm{p} = 100$ µm.

The numerical set-up which we used for this study is visualized in figure 3(a). The domain of interest is a cube whose edges have a length of 8 cm. If a particle collides with the wall it is reflected. In order to focus on the interaction between particles, neither charged was exchanged during wall collisions nor induced charges at the walls were taken into account. Thus, the kinetic energy of the particle remained constant during the collision. In the simulation shown in figure 3 512 particles of the properties $\varphi = 10^6\ \Omega$ m, $\gamma = 8.4 \times 10^{-7}$ m s^2/kg and $\rho_\mathrm{p} = 4000$ kg/m^3 were released, resulting in a number density of $\rho = 1$ cm^{-3}. Initially ($t = 0$ s, figure 3(a)) the particles were distributed with an equal spacing between each other. While the amplitude of the initial velocity was the same for all particles, the direction of the velocity vector of the particles was ascribed randomly. In order to mimic a scenario similar to the real situation in a flow, the particles initially located at the bottom half of the domain were charged whereas those at the top half were uncharged. This idealizes the situation of particles residing close to the wall and gaining charge and other particles being located in the bulk of the flow. The initial charge of the charged particles is denoted by Q_max which is 1 pC in the case of figure 3.

The particle positions and their charge after a computation time of 0.05 s is given in figure 3(b). Here, the majority of the charge is retained in the bottom of the domain. However, at the interface region between the charged and uncharged particles, a charge mixing layer is formed. A few particles in this layer exhibit charges between zero and Q_max which indicates charge redistribution through collisions of charged and uncharged particles. Further, figure 3(c) shows the situation after $t = 0.5$ s. Here, the charge is apparently mixed rather homogeneously in the domain which suggests an effective inter-particle charge diffusion.

In order to gain further insight in the charge redistribution process, the probability density function (pdf) of the particle charge is plotted for several time instances in figure 4(a). For the time instance of $t = 0.01$ s, i.e. shortly after the beginning of the simulation, two charge peaks can be observed, one representing the uncharged particles at the top and one representing the particles at the bottom charged with Q_max. After 0.6 s the particles exhibit a wide range of charges between zero and Q_max. The pdf relating to the time instance $t = 1.4$ s formed a peak at $Q = Q_\mathrm{max}/2 = 0.5$ pC which corresponds to the average initial charge of the total ensemble of particles. At $t = 2$ s this peak grows close to double the value of the initial charge peaks, indicating that nearly all particles in the domain reached an equilibrium charge. In other words, the charge is homogeneously distributed via inter-particle charge diffusion.

For comparison purposes, in figure 4(b) the pdfs at the same time instances are plotted. All parameters of this case are identical to the previous one, except φ was increased to $10^7\ \Omega$ m. Contrary to the previous observations, in this case the charge is distributed among particles in a much slower rate and even after 2 s no distinct peak is formed at $Q = 0.5$ pC. Reason is the increase of the charge relaxation time which comes along with an increase in φ, cf. equation (8). Therefore, a smaller part of the total particle charge is transferred during a collision for $\varphi = 10^7\ \Omega$ m compared to $\varphi = 10^6\ \Omega$ m. It is emphasized that also for the latter case the final distribution will have a single peak at $Q = 0.5$ pC, but it takes much longer.

In order to provide a measure of the homogeneity of the pdfs in figure 4, the root mean square (rms) of the charge distributions is defined as

$$Q_\mathrm{rms} = \left(\frac{1}{N} \sum_{i=1}^{N} \left| Q_i - \bar{Q} \right|^2 \right)^{1/2}, \qquad (15)$$

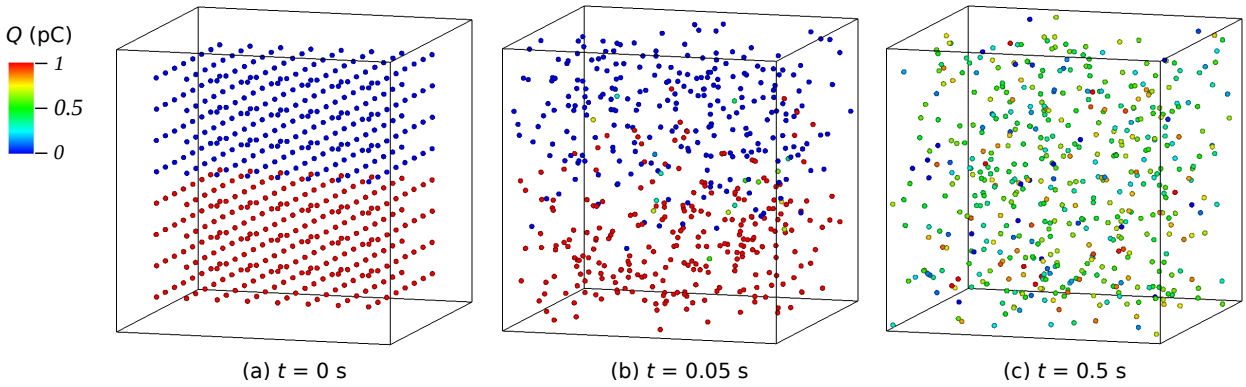

Figure 3: Instantaneous snapshots of the computations of 512 particles released in a cube of the side length of 8 cm, i.e. $\rho = 1$ cm^{-3}. Figure (a) shows the initial condition. After 0.05 s (b) few particles exchanged charge through collisions. Moreover, after 0.5 s (c) the charge is rather homogeneously distributed through inter-particle charge diffusion. The considered conditions are $\varphi = 10^6\ \Omega$ m, $\gamma = 8.4 \times 10^{-7}$ m s^2/kg, $Q = 1$ pC and $\rho_\mathrm{p} = 4000$ kg/m^3.

where $\bar{Q}$ denotes the average particle charge. Since during collisions between particles no charge is generated or destroyed, $\bar{Q}$ remains constant during the computation and equals $Q_\mathrm{max}/2$. The time evolution of Q_rms for the discussed cases is plotted in figure 5. Additionally, the results of a case with $\varphi = 10^6\ \Omega$m and a reduction of gamma to $\gamma = 8.4 \times 10^{-8}$ m s^2/kg is shown. The curves confirm the previous observation that the rms drops faster, i.e. the charge distributes faster, if φ is reduced. Further, the charge distribution is reduced if γ is decreased. This can be explained by the fact that a reduction of γ results in a reduction of the contact area during collisions between particles, cf. equations (9) and (10). Thus, less charge is exchanged during each collision.

Interestingly, the rms plots shown in figure 5 resemble closely an exponential decay function of the shape

$$Q_\mathrm{rms} = Q_\mathrm{0,rms}\, \mathrm{e}^{-t/\tau}\,. \tag{16}$$

In the above equation, $Q_\mathrm{0,rms}$ is the initial rms value which can be determined from the initial charge distribution to be equal to $Q_\mathrm{max}/2$. Further, τ is the time scale of the decay, which was approximated from the numerical results as the time when Q_rms drops to the value $Q_\mathrm{0,rms}$/e. Using this definition, time scales of $\tau = 0.64$ s, 2.48 s and 1.72 s were measured where the second value corresponds to the case of $\varphi = 10^7\ \Omega$m and the third value to the case of $\gamma = 8.4 \times 10^{-8}$ m s^2/kg. The decay functions are also plotted in figure 5. Evidently, τ can be interpreted as a time-scale that characterizes the efficiency of inter-particle charge diffusion. The smaller it is, the more efficient the charge transferred via inter-particle collisions becomes. Therefore, τ can be used as a measure to evaluate the importance of this mechanism for different conditions.

In the following, the second and third group of parameters is investigated, i.e. the parameters that influence the particle interactions and the type of interaction, namely ρ, ρ_p and Q whereas r_p and u_0 were kept constant as discussed above. Also, φ and γ are kept constant at $10^6\ \Omega$m and 8.4×10^{-7} m s^2/kg, respectively. With this choice of values the expected time scales were low and, therefore, the computation times limited.

Figure 6 shows the influence of the particle number density on τ for two different particle material densities. An increase in ρ_p leads to a higher particle kinetic energy and, thus, more severe collisions and, consequently, more charge exchange and in general smaller values for τ. Moreover, a higher number density leads to a higher collision frequency which also results in smaller decay times. Asymptotically, τ seems to approach zero for a further increase in ρ, i.e. for a very high particle number density inter-particle charge diffusion occurs almost instantly. On the contrary, at low number densities no collisions take place and, therefore, τ grows asymptotically.

The influence of the particle material density on τ is further explored in figure 7. This figure shows results at the same data points as in the previous figure whereas the asymptotic behavior of τ for further density reductions is investigated. By showing the curves for two different particle number densities, we demonstrate that the aforementioned relationship for the decay time scale holds for a wide range of particle material densities. The increase of the decay time scale is even more pronounced when the particle material density is reduced

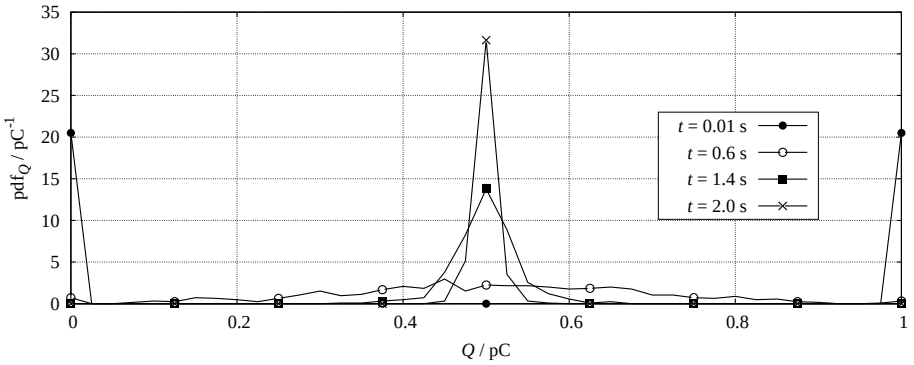

(a)

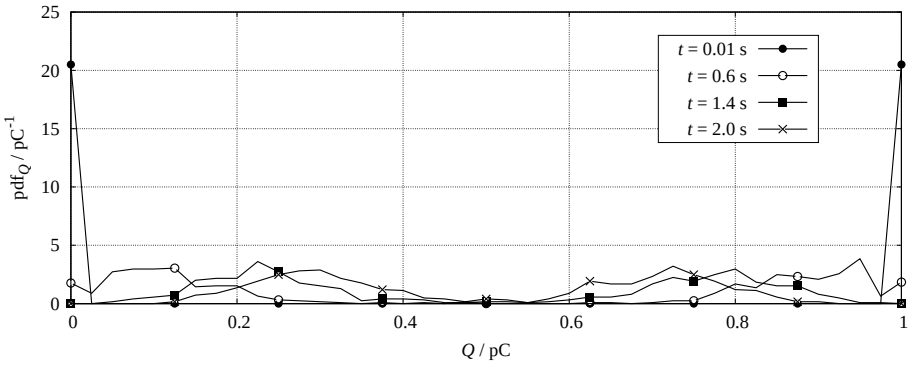

(b)

Figure 4: Evolution of the probability density function (pdf) of the particle charge for several time instances. Figure (a) relates to particles of $\varphi = 10^6\ \Omega\,\mathrm{m}$ whereas figure (b) relates to $\varphi = 10^7\ \Omega\,\mathrm{m}$. The other parameters of both simulations are identical, i.e. $\gamma = 8.4 \times 10^{-7}\ \mathrm{m\,s^2/kg}$, $\rho_\mathrm{p} = 4000\ \mathrm{kg/m^3}$ and $\rho = 1\ \mathrm{cm^{-3}}$.

to 250 kg/m^3 and 62.5 kg/m^3. In these cases the inertial energy of the system is further reduced. If the particles experienced one or a few collisions they accumulate charge which is sufficient to prevent further collisions. An interesting region in the figure, with respect to inter-particle charge diffusion, can be identified around the data points for $\rho = 3.375\ \mathrm{cm^{-3}}$ and intermediate material densities of $\rho_\mathrm{p} = 250\ \mathrm{kg/m^3}$ and $1000\ \mathrm{kg/m^3}$. Here, τ is low due to the high particle number density, thus, inter-particle charge diffusion is effective. At the same time, the particles' inertia is low which means that for these conditions inter-particle charge diffusion might be the dominating mechanism to transport charge in space. For the same number density but higher values of ρ_p inter-particle charge diffusion is still effective, however, here particle-bound charge transfer is expected to be more important.

Finally, the influence of the initial particle charge on the charge transfer is evaluated. To this end, the decay time scales for variations of Q_max from 0.01 pC to 3000 pC is plotted in figure 8. It can be seen that for initial charges of up to 100 pC τ is independent of Q_max. However, for higher initial charges the decay time scale reduces steadily.

In order to identify the reason for this behavior, the cases of initial charges of 100 pC and 2000 pC are further analyzed in figure 9. For the initial charge of 100 pC it can be observed that the average specific kinetic energy of the particle ensemble, e_kin, is constant $0.127\ \mathrm{m^2/s^2}$ which is very close to the value given to the particles by their initial velocity. The average particle collision frequency is low during the first 0.02 s which is related to the uniform initial spacing of the particles and the finite initially assigned velocity and charge. Afterwards, the frequency remains in a band below $5\ \mathrm{s^{-1}}$. On the contrary, the average specific kinetic energy of the case of an initial charge of 2000 pC rises fast above $1\ \mathrm{m^2/s^2}$. This is related to the potential electrostatic en-

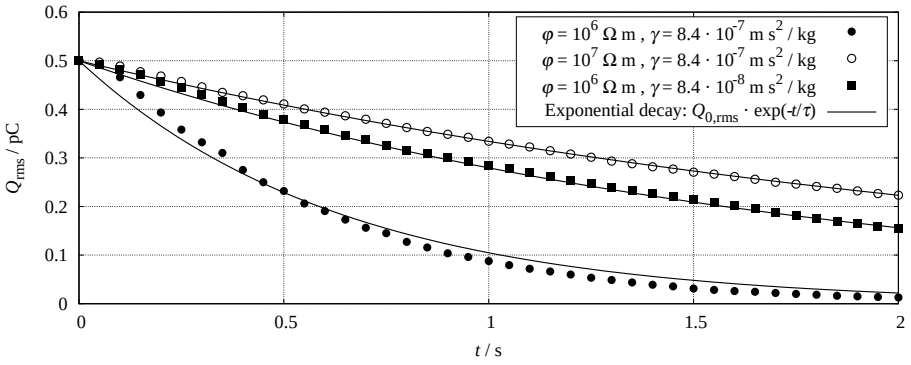

Figure 5: The time evolutions of the rms of the charge distribution resemble closely an exponential decay function. The three plotted cases relate to particles of $\gamma = 8.4 \times 10^{-7}$ m s^2/kg, $\rho_\mathrm{p} = 4000$ kg/m^3 and $\rho = 1$ cm^{-3}.

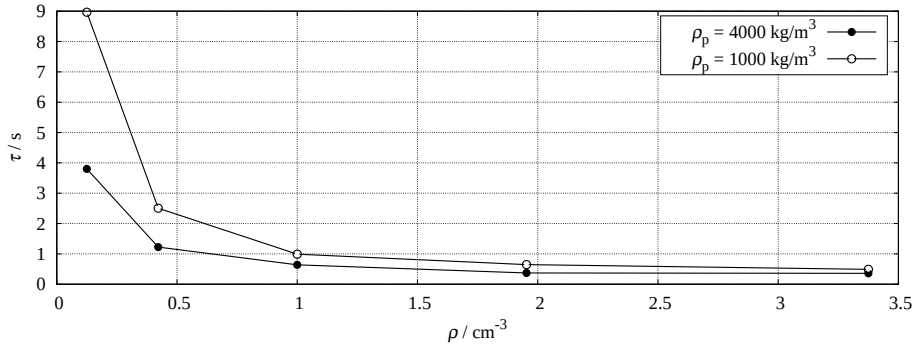

Figure 6: Decay time scale versus particle number density. The considered conditions are $\varphi = 10^6\ \Omega$ m, $\gamma = 8.4 \times 10^{-7}$ m s^2/kg and $Q = 1$ pC.

ergy due to the higher initial charge. Since this charge is spatially uneven distributed, the electric field accelerates the charged particles towards the uncharged, thus, transforming potential into kinetic energy. Due to this increase also the collision frequency significantly increases as it can be inferred from figure 9. Thus, af-

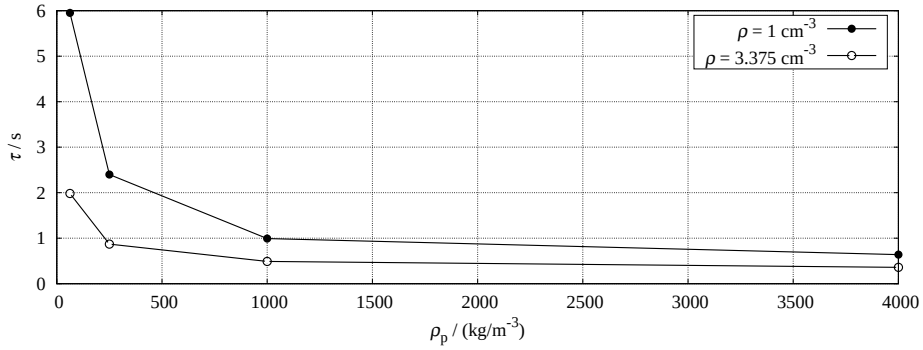

Figure 7: Decay time scale versus particle material density. The considered conditions are $\varphi = 10^6\ \Omega$ m, $\gamma = 8.4 \times 10^{-7}$ m s^2/kg and $Q = 1$ pC.

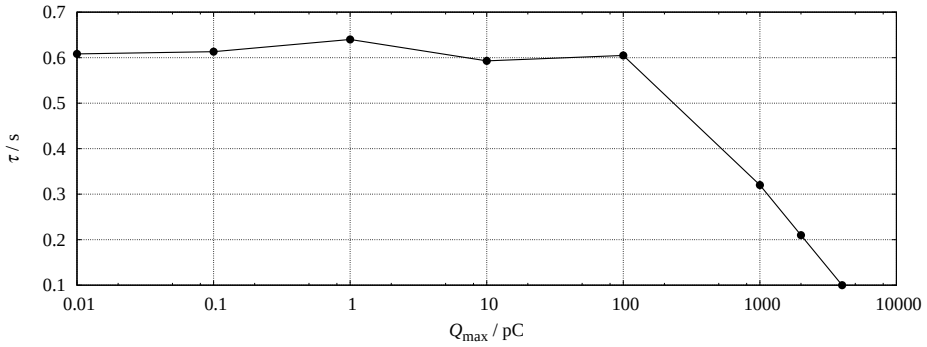

Figure 8: Decay time scale versus maximum particle charge. The considered conditions are $\varphi = 10^6\ \Omega\,\mathrm{m}$, $\gamma = 8.4 \times 10^{-7}\ \mathrm{m\,s^2/kg}$, $\rho = 1\ \mathrm{cm^{-3}}$ and $\rho_\mathrm{p} = 4000\ \mathrm{kg/m^3}$.

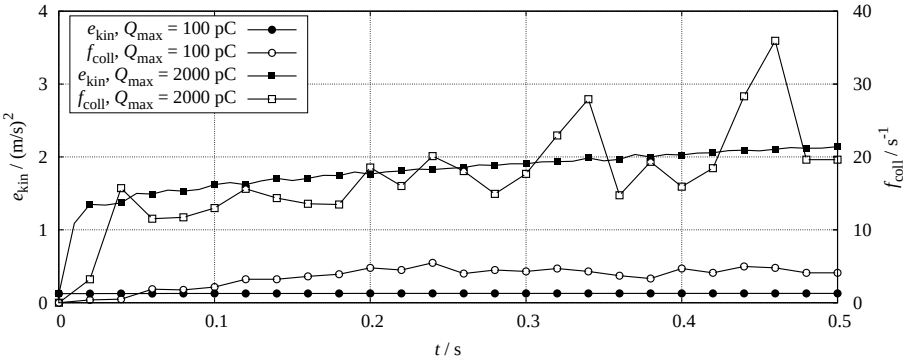

Figure 9: Time evolution of the average specific kinetic energy and the average collision frequency of the particles. The considered conditions are $\varphi = 10^6\ \Omega\,\mathrm{m}$, $\gamma = 8.4 \times 10^{-7}\ \mathrm{m\,s^2/kg}$, $\rho = 1\ \mathrm{cm^{-3}}$ and $\rho_\mathrm{p} = 4000\ \mathrm{kg/m^3}$.

ter a certain threshold, which is here 100 pC, the initial charge enhances both inter-particle charge diffusion and particle-bound charge transfer. In other words, if particles accumulate a high charge at a wall, i.e. because of a high contact potential, the arising electric field supports the transport of the charge towards the bulk of the flow.

4. Conclusions

In this paper we investigated numerically the mechanism of inter-particle charge diffusion in particulate flows. In order to evaluate the efficiency of the studied mechanism a time scale characterizing the charge redistribution was proposed. Through a generic set-up fundamental insight in the influence of various parameters on the charge transfer was obtained. The main conclusion of the study is that a high particle number density, particle material density or particle charge leads to a fast charge redistribution and accordingly a low characteristic time. Given the importance of wall-normal charge transport, this results aid the further understanding of the electrification of fluid-solid mixtures. The information concerning the characteristic time scale may be utilized in the future to define a diffusion coefficient, analogous to other diffusion processes.

References

J. G. Tralles. *Beytrag zur Lehre von der Elektrizität*. Haller, 1786.

P. Lenard. Über die Elektrizität der Wasserfälle. *Ann. Phys.*, 46:584–636, 1892.

A. Klinkenberg and J. L. van der Minne. *Electrostatics in the Petroleum Industry*. Elsevier Publ. Co., 1958.

H. Krämer. Kriterien zur Beurteilung der Zündgefahren infolge elektrostatisch aufgeladener Flüssigkeiten. *Chem. Ing. Tech.*, 55:419–428, 1983.

H. Grosshans and M. V. Papalexandris. Direct numerical simulation of triboelectric charging in a particle-laden turbulent channel flow. *J. Fluid Mech.*, 818:465–491, 2017a.

W. R. Harper. The Volta effect as a cause of static electrification. *Proc. Royal Soc. London Series A*, 205:83–103, 1951.

J. Lowell and A. R. Akande. Contact electrification–why is it variable? *J. Phys. D: Appl. Phys.*, 21:125–137, 1988.

T. Matsuyama and H. Yamamoto. Charge relaxation process dominates contact charging of a particle in atmospheric conditions. *J. Phys. D: Appl. Phys.*, 28:2418–2423, 1995.

T. Matsuyama and H. Yamamoto. Charge relaxation process dominates contact charging of a particle in atmospheric conditions: II. The general model. *J. Phys. D: Appl. Phys.*, 30:2170–22175, 1997.

P. Ireland. The role of changing contact in sliding triboelectrification. *J. Phys. D: Appl. Phys.*, 41:025305, 2008.

S. L. Soo. Dynamics of Charged Suspensions. In *Topics in Current Aerosol Research*, pages 71–73. Pergamon Press, 1971.

R. G. Harrison, E. Barth, F. Esposito, J. Merrison, F. Montmessin, K. L. Aplin, C. Borlina, J. J. Berthelier, G. Déprez, W. M. Farrell, I. M. P. Houghton, N. O. Renno, K. A. Nicoll, S. N. Tripathi, and M. Zimmerman. Applications of electrified dust and dust devil electrodynamics to martian atmospheric electricity. *Space Sci. Rev.*, 203:299–345, 2016.

G. E. Bowker and H. C. Crenshaw. Electrostatic forces in wind-pollination–part 1: Measurement of the electrostatic charge on pollen. *Atmos. Environ.*, 41:1587–1595, 2007.

H. Grosshans and M. V. Papalexandris. Evaluation of the parameters influencing electrostatic charging of powder in a pipe flow. *J. Loss Prev. Process Ind.*, 43:83–91, 2016a.

H. Grosshans and M. V. Papalexandris. Large eddy simulation of triboelectric charging in pneumatic powder transport. *Powder Technol.*, 301:1008–1015, 2016b.

H. Grosshans and M. V. Papalexandris. A model for the non-uniform contact charging of particles. *Powder Technol.*, 305:518–527, 2016c.

H. Grosshans and M. V. Papalexandris. Numerical study of the influence of the powder and pipe properties on electrical charging during pneumatic conveying. *Powder Technol.*, 315:227–235, 2017b.

N. Schwindt, U. von Pidoll, D. Markus, U. Klausmeyer, M. V. Papalexandris, and H. Grosshans. Measurement of electrostatic charging during pneumatic conveying of powders. *J. Loss Prev. Process Ind.*, 49:461–471, 2017.

M. Caporaloni, F. Tampieri, F. Trombetti, and O. Vittori. Transfer of particles in nonisotropic air turbulence. *J. Atmos. Sci.*, 32:565–568, 1975.

M. W. Reeks. The transport of discrete particles in inhomogeneous turbulence. *J. Aerosol Sci.*, 14:729–739, 1983.

P. J. Roache. Quantification of Uncertainity in Computational Fluid Dynamics. *Annu. Rev. Fluid Mech.*, 29:123–160, 1997.

R. Brück. Chemische Konstitution und elektrostatische Eigenschaften von Polymeren. *Kunststoffe*, 71:308–312, 1981.

A. R. Akande and J. Lowell. Charge transfer in metal/polymer contacts. *J. Phys. D: Appl. Phys.*, 20:565–587, 1987.

H. T. Baytekin, M. Patashisnki, A. Z. Branicki, B. Baytekin, S. Soh, and B. A. Grzybowski. The mosaic of surface charge in contact electrification. *Science*, 33:308–312, 2011.

H. Grosshans and M. V. Papalexandris. On the accuracy of the numerical computation of the electrostatic forces between charged particles. *Powder Technol.*, 322:185–194, 2017c.